applied sciences

MDPI

Article

Archaeometric Surveys of the Artifacts from the Archaeological Site of Baro Zavelea, Comacchio (Ferrara, Italy)

Elena Marrocchino [1,*], Chiara Telloli [2], Umberto Tessari [3], Mario Cesarano [4], Marco Bruni [5] and Carmela Vaccaro [1,6]

[1] Department of Environmental and Prevention Sciences, University of Ferrara, Corso Ercole I d'Este, 32, 44121 Ferrara, Italy
[2] ENEA, Italian National Agency for New Technologies, Energy and Sustainable Economic Development Fusion and Technology for Nuclear Safety and Security Department Nuclear Safety, Security and Sustainability Division, Via Martiri di Monte Sole 4, 40129 Bologna, Italy
[3] Department of Physic and Earth Sciences, University of Ferrara, Via Saragat 1, 44122 Ferrara, Italy
[4] Ministry of Culture, Superintendence Archaeology, Fine Arts and Landscape of Naples Metropolitan Area, 80135 Napoli, Italy
[5] Excogita di Bruni Marco, Via Nino Bixio 18, 44020 Stellate, Italy
[6] ISAC-CNR Institute of Atmospheric Sciences and Climate of the National Research Council of Italy, 40129 Bologna, Italy
* Correspondence: mrrlne@unife.it; Tel.: +39-33-938-07477

Abstract: This work is part of a project of the Superintendence of Archaeology, Fine Arts, and Landscape for the enhancement of the widespread archaeological heritage of the Po delta area. Excavation activities, carried out in 2015, allowed the sampling of the stratigraphic elements and artifacts of the archaeological site of the lighthouse tower of Baro Zavelea, municipality of Comacchio (Ferrara, northeast Italy). In this work, the geochemical characterization of sediments and building materials was conducted using granulometric analyses, X-ray fluorescence analysis, and calcimetry on different types of samples, including sands, clays, mortars, and bricks, with the scope to better characterize all of the different types of sediments collected. This multidisciplinary approach allowed the diagnostic and evaluation of the state of conservation of Baro Zavalea. Granulometric analyses highlighted the fact that depositional environments were of very different natures: fluvial environments and paleo–alveo environments. In addition, XRF analysis allowed the discrimination of different clay samples, some from basins poor in carbonates, while, for the construction of the bricks of the second wall structure, clays rich in carbonate were chosen to add lightness to the structure.

Keywords: petroarchaeometric characterization; XRF; bricks; mortars; clay; sand; Baro Zavelea; comacchio

Citation: Marrocchino, E.; Telloli, C.; Tessari, U.; Cesarano, M.; Bruni, M.; Vaccaro, C. Archaeometric Surveys of the Artifacts from the Archaeological Site of Baro Zavelea, Comacchio (Ferrara, Italy). *Appl. Sci.* **2022**, *12*, 11692. https://doi.org/10.3390/app122211692

Academic Editor: Theodore E. Matikas

Received: 15 October 2022
Accepted: 16 November 2022
Published: 17 November 2022

1. Introduction

This research work arises from the perfect combination of archaeology and science—archaeometry and sedimentology have played a fundamental role in the acquisition of useful data for the reconstruction of an archaeological excavation [1].

There have been many scientific types of research aimed at characterizing excavation contexts and artifacts, such as ceramics and bricks [2,3]. The latter constitute most of the findings in archaeological excavations, and many involved researchers who have provided various contributions aimed at the mineralogical, chemical, and petrographic characterization of these materials [4–6].

Discriminating and characterizing the origin of the sediments present in a specific site is fundamental and it is, generally, one of the first research stages undertaken by archaeologists, as clay and sand are the raw materials from which historical artifacts and construction materials were made [7,8].

Even the sands and clays of the river Po (north Italy) have often been studied as raw materials for the construction of historical buildings and ancient objects found in archaeological excavations [9]. The river Po has always played an important role in history, both as a navigation channel [10] and also as a source of raw materials for construction [9].

The branches of the Po delta were described by Pliny proceeding along the Adriatic coast from south to north. These branches, in the southern sector of the delta, could be divided into four parts [11], including the Fossa Augusta and Padusa canals. This part of the Po delta belonged to the southernmost branch that was already fossilized in Roman times and was partially revitalized by the construction of the Fossa Augusta. The navigable canal detached from Padovetere in the locality of Baro Zavelea, reached the Padusa canal and, together with it, flowed into the port of Ravenna, where the imperial fleet was stationed and, therefore, resized in the Augustan period. This port installation was fundamental on a military, commercial, and supply level.

The area of Baro Zavelea refers to the wreck of a coastal strip that emerged in the Mezzano valley west of the Padovetere. During the Roman period, especially in the Augustan age, this stretch was affected by the crossing of the Fossa Augusta. The Augustan navigable canal branched off on the southern branch of the Po, north of the Church of Santa Maria in Padovetere [12], perhaps near the locality of Casone Paviero–Bocca delle Menate, and then headed toward Casone Bingotta–Via Anita [13]. Once the area of Baro Zavelea was intercepted, the canal entered the Argine d'Agosta and then reached Ravenna in the final part of its route. Both the Argine d'Agosta and Baro Zavelea, during the excavation of drainage channels for reclamation works, were the subjects of archaeological investigations that brought to light several sites of considerable interest, including Villa di Salto del Lupo investigated in the 1960s and a lighthouse tower located in Baro Zavelea, the object of study of this work [13].

In the Roman period, the river bumps close to the delta ramifications and the coastal strips that proceeded along the same direction as the beach line were the main places where the population was distributed [13]. These were the only areas suitable for settlement due to the elevated position, because, in its terminal part, the delta landscape was formed from swamps and marshes [14,15].

The archaeological site of the lighthouse tower of Baro Zavelea, the object of study of this work, is located near the Municipality of Comacchio in the province of Ferrara and, between 1965 and 1978, was the subject of numerous excavation campaigns that allowed different settlements to be highlighted. In detail, in August 1976, the first excavation campaign was carried out in the Baro Zavelea area because, during the plowing work by peasants in the neighboring lands, numerous sesquipedalian bricks came to light, which prompted the archaeologists to promptly excavate the area [13]. During the subsequent campaign conducted in September 1976, an imposing square base of 7.42 m wide and 2 m high was found resting on a square platform contained by a double piling of oak logs, which formed a square of about 10 m sideways [12]. The structure consisted entirely of sesquipedalian bricks bonded with white mortar composed of coarse-grained sand.

From the very beginning, archaeologists have advanced the hypothesis that it could be a lighthouse tower, given the presence of many erratic bricks found in the excavation area that confirm the considerable original height of the monument. Based on the size of the base and taking into account the number of erratic bricks recovered in the 1970s and the subsequent excavation campaign (2015), it is plausible to believe that, originally, it could have reached a height of 25 feet, typical of early age imperial towers [12].

In 2015, the Superintendence of Archaeology, Fine Arts, and Landscape decided to investigate the area again. The campaign allowed objects of considerable importance and an equally interesting context of excavation to be found. The excavation activities allowed the sampling of the stratigraphic elements and the artifacts of the archaeological site of the Baro Zavelea lighthouse tower.

This work aimed to better characterize all of the sediments collected and some fragments of the bricks of the lighthouse tower through geochemical analyses. Granulometric analyses, X-ray fluorescence analysis, and calcimetric analysis were conducted on several types of samples (sands, clays, mortars, and bricks).

2. Materials and Methods

2.1. Sampling Site Description

In the Baro Zavelea area, located in the municipality of Comacchio in the province of Ferrara (Emilia Romagna region, northeast Italy–Figure 1a), there are remains of a lighthouse tower that have been investigated through different excavation campaigns. The last of these was divided into different phases:

- The first phase was completely dedicated to the excavation of the lighthouse tower built entirely of rectangular (45 × 30) sesquipedalian bricks (Figure 1b). During the sampling, some sesquipedalian bricks equipped with a handle were also found, which were probably used to allow for easier hand transport. The first phase of excavation also investigated the 8 foundation piles that emerged covered by a considerable layer of clay and were subsequently sampled for analysis (Figure 1c);
- In the subsequent phases, a large part of the area located to the east was investigated, in which important finds were found, as well as a second wall structure consisting of bricks characterized by considerable fragility and different colors (from yellow to purple), probably due to different cooking temperatures (Figure 1d). The wall structure rested on a wooden grid and had two foundation cuts on the sides with bricks placed transversely. The wooden grid was not unusual in the Po delta area, similar to that found during the excavations of the Etruscan Spina [16], where structures of this type were necessary given the confirmation of the territory characterized by a lot of marshes.

In addition to the second wall structure found, a high number of fragments of slabs and a parallelepiped in white stone weighing two tons were found in the collapse/dispossession layer. The layer defined as "collapse/dispossession" was littered with bricks and stones, interspersed with a very high number of shells ascribable to both fresh and salt water. Additionally, a few ceramic fragments were found that chronologically date back to the 4th–5th century AD (Figure 1e,f).

At the northeast end of the excavation area, a large block of white stone was found (Figure 1g,h), decorated in bas-relief on three sides, which, for the decorative motifs, was placed in the Julius–Claudian age (30–50 AD). On the block, there was a hole that probably held a statue (Figure 1g).

Adding to these samples, other white stone slabs were found (6 in all), some of which were characterized by the presence of holes (Figure 1i).

Figure 1. Picture of the sampling site: (**a**) Comacchio in the Emilia Romagna region on the Adriatic Sea—the excavation area of Baro Zavelea is in the red circle; (**b**) view of the excavation area; (**c**) foundation piles; (**d**) detail of the wooden grid; (**e**) example of ceramic fragments; (**f**) amphora; (**g**) large block of white stone decorated in bas-relief; (**h**) detail of the large block; (**i**) white stone slabs.

2.2. Sampling Methodology and Analytical Techniques

The sampling was planned to better characterize the sedimentological, stratigraphic, and constructive context that emerged during the excavation campaign conducted in 2015.

Different kinds of samples (bricks, mortars, clays, sands, and trachyte samples) were collected and analyzed in the laboratories of the Department of Physics and Earth Sciences of the University of Ferrara. Table 1 describes the collected provenance for each type of sample analyzed.

Table 1. Description of the different kinds of samples collected and analyzed, and the descriptions of the provenance of each sample.

Sample	Description	Provenance
1	Brick	Lighthouse tower remains
2	Brick	Lighthouse tower remains
3	Brick	Second wall structure
4	Brick	Second wall structure
5	Brick	Second wall structure
6	Brick	Second wall structure
7	Brick	Second wall structure
8	Brick	Second wall structure
9	Mortar	Lighthouse tower remains
10	Mortar	Lighthouse tower remains
11	Mortar	Second wall structure
12	Mortar	Second wall structure
13	Mortar	Second wall structure
14	Mortar	Second wall structure
15	Mortar	Second wall structure
16	Mortar	Second wall structure
17	Mortar of the collapse	Second wall structure
18	Clay	Clay layer

19	Clay	Clay layer
20	Sand	East part of the excavation area
21	Sand	East part of the excavation area
22	Sand	East part of the excavation area
23	Sand	East part of the excavation area
24	Sand	East part of the excavation area
25	Sand	North part of the excavation area
26	Sand	North part of the excavation area
27	Sand	North part of the excavation area
28	Sand	Second wall structure
29	Sand	South part of the excavation area
30	Sand	South part of the excavation area
31	Sand	South part of the excavation area
32	Sand	South part of the excavation area
33	Sand	South part of the excavation area
34	Sand	South part of the excavation area
35	Sand	South part of the excavation area
36	Trachyte	South part of the excavation area
37	Trachyte	South part of the excavation area

Particle size analyses were performed on 24 samples, which were chosen based on any anthropogenic influence or natural deposition, dividing the samples into two classes: mortars (from sample 10 to sample 17) and sediments of natural origin (samples 20 to 35).

Samples were initially quartered to obtain a representative amount to be analyzed and then treated with a low concentration (16 vol) of hydrogen peroxide to oxidize the organic matter and achieve a good dispersion of clasts. Once the oxygenation phase was considered complete, the sandy fraction was separated from the muddy one by wet sieving using a 63 μm net. The muddy fraction was collected in plastic jugs and left to settle completely.

The sandy fraction, placed in glass beakers, was dried in an oven at a temperature of 60 °C for at least 24 h. Once dried, any bioclasts with dimensions larger than the coarser clasts were eliminated by manual sieving using sieves of a suitable mesh size. Subsequently, the sediment was weighed on a technical scale to the centigram to determine its net weight.

The mud, after the elimination of the excess water contained in the jugs by siphoning, was recovered into a pre-weighed beaker. After further sedimentation and elimination of excess water, the mud was weighed and, through a 60 °C L.O.I. performed on a small amount, the whole net dry weight of the fraction was calculated. This procedure was adopted to avoid possible granulometric alterations of the muddy fraction due to its drying and subsequent rehydration.

A representative portion of the sandy fraction (2.8–3.2 g) was analyzed using a sedimentation tube consisting of a plate connected to a balance and immersed in a sedimentation apparatus [17] that can measure particle dimensions by Stokes Law.

The muddy fraction was analyzed using a Micromeritics Sedigraph with a sodium hexa-metaphosphate solution (concentration 0.5%) as a dispersant liquid. Even the Micromeritics Sedigraph based its measurement principle on Stokes' law [18].

The analytical data from both instruments were then merged, in proportion to the relative abundances of the two respective fractions, using the Sedimcol software (version 1.06), obtaining the entire particle size distribution for each sample analyzed. Cumulative curves, Wentworth [19] classification, and Folk and Ward [20] parameters were obtained.

All the samples were analyzed by X-ray fluorescence (XRF). Before analysis, all of the samples were ground into a powder with a particle size of less than 2 μm using a Power Mortar Grinder MG100 Vibration Mill (Laarman, Maribor, Slovenia).

The sample powders were first dried in an oven at 110 °C, then placed in ceramic crucibles and subjected to a temperature of 1000 °C for one day [10]. Part of the powder

from all of the samples was used for L.O.I. (loss on ignition) calculation and expressed in Table 2 as the weight oxide percentage. An amount of 0.5 g of powder for each sample was prepared by pressing a tablet on boric acid support for XRF analysis. The chemical analysis of the collected fragments was determined by XRF with a wavelength dispersion spectrometer ARL Advant-XP (Thermo Fisher Scientific, Waltham, MA, USA) [21]. The instrument consisted of an X-ray tube with a Mo target and an SSD Peltier-cooled detector (10 mm^2 active area and resolution of <155 eV at 10 kcps). The system performs a simultaneous multi-element analysis in the element range from Na (11) to U (92). A maximum voltage and current of 50 kV and 1500 μA, respectively, were used to excite the secondary fluorescence X-rays. A collimator with a diameter of 1 mm was used to collect the emitted secondary X-rays from a surface area of about 0.79 mm^2 in the air [22]. This technique allowed the determination of the major elements, expressed as a percentage by oxide weight (SiO_2, TiO_2, Al_2O_3, Fe_2O_3, MnO, MgO, CaO, Na_2O, K_2O, and P_2O_5), and of the following trace elements reported in ppm (parts per million): Ba, Cr, Ni, Pb, Rb, Sr, V, Zn, Zr, Nd, and S [23]. The accuracy of the instrument, estimated based on the results obtained for international standards of geological samples, and the precision, expressed as the standard deviation of replicated analyses, were between 2% and 5% for the major elements and between 5% and 10% for trace elements. The detection limit (0.01% for major oxides) was estimated to be close to ppm for most trace elements, except for S, for which a detection limit of 50 ppm was considered. The processing of the acquired intensities and the correction of the matrix effect were performed according to the model proposed by Lachance and Trail [24]. The qualitative data obtained were expressed as the single element weight.

Table 2. XRF data of the major oxides present in the samples collected and expressed in weight (%).

(a)					**Bricks**				**Clays**	
	1	**2**	**3**	**4**	**5**	**6**	**7**	**8**	**18**	**19**
SiO_2	51.58	54.11	55.50	55.49	56.19	52.47	53.74	53.94	68.21	64.73
TiO_2	0.65	0.66	0.81	0.66	0.77	0.67	0.66	0.69	0.23	0.22
Al_2O_3	12.39	14.38	16.33	14.56	15.27	12.86	14.43	13.74	8.71	9.06
Fe_2O_3	5.55	6.04	6.49	6.06	6.25	5.56	6.40	6.29	2.14	2.13
MnO	0.12	0.14	0.13	0.12	0.14	0.12	0.13	0.14	0.04	0.07
MgO	5.13	5.65	4.12	5.93	4.41	4.10	4.29	4.30	3.37	3.81
CaO	17.03	13.39	9.28	11.77	10.55	15.95	15.29	16.17	8.65	11.18
Na_2O	2.41	2.03	1.26	2.06	1.72	1.92	3.27	2.77	2.01	1.76
K_2O	1.24	1.98	2.75	2.12	2.54	2.30	1.00	0.94	2.26	2.21
P_2O_5	0.55	0.20	0.33	0.23	0.21	0.33	0.14	0.34	0.11	0.14
L.O.I.	3.36	1.42	2.99	0.99	1.96	3.72	0.64	0.67	4.26	4.69
Carbonate Content	8					6			8	2
Tot	100	100	100	100	100	100	100	100	100	100
(b)					**Mortars**				**Trachyte**	
	9	**10**	**11**	**12**	**13**	**14**	**15**	**16**	**17**	**36**	**37**
SiO_2	58.30	57.65	61.25	63.19	54.88	54.64	53.36	61.54	66.06	57.10	62.25
TiO_2	0.46	0.26	0.22	0.21	0.24	0.21	0.23	0.55	0.60	0.73	0.69
Al_2O_3	10.35	8.69	8.93	8.96	7.79	7.47	7.93	11.46	9.35	18.82	14.23
Fe_2O_3	3.29	2.34	2.17	2.07	2.29	1.95	2.30	3.92	4.03	7.30	5.62
MnO	0.09	0.05	0.06	0.07	0.07	0.08	0.08	0.09	0.13	0.04	0.05
MgO	4.20	3.56	3.69	3.66	2.90	2.79	3.05	5.18	4.83	5.42	5.29
CaO	12.03	14.86	12.62	11.86	18.47	18.16	19.25	8.63	7.66	1.07	4.42
Na_2O	1.49	1.61	1.66	2.06	1.51	1.71	1.78	1.68	1.88	1.79	1.34
K_2O	2.06	2.04	2.10	2.23	1.91	1.80	1.94	2.19	1.71	3.52	2.62
P_2O_5	0.16	0.12	0.14	0.12	0.16	0.14	0.15	0.26	0.14	0.15	0.32
L.O.I.	7.56	8.82	7.18	5.56	9.79	11.06	9.92	4.48	3.60	4.07	3.16

Carbonate Content	19								16		19	21	6			
Tot	100		100		100	100	100		100		100	100	100		100	100
(c)	**20**	**21**	**22**	**23**	**24**	**25**	**26**	**27**	**28**	**29**	**30**	**31**	**32**	**33**	**34**	**35**
SiO_2	66.37	62.04	58.85	58.40	60.72	53.62	54.60	56.30	58.08	60.43	59.86	59.54	65.87	59.80	55.90	57.77
TiO_2	0.71	0.64	0.66	0.78	0.72	0.71	0.67	0.89	0.67	0.66	0.62	0.63	0.93	0.50	0.79	0.82
Al_2O_3	10.17	13.09	14.42	9.62	13.19	14.33	14.43	16.37	11.59	13.23	11.59	12.03	10.37	13.04	15.77	15.33
Fe_2O_3	4.01	4.64	5.64	4.91	5.34	5.18	5.11	6.88	4.30	5.17	4.47	4.43	5.85	7.75	6.72	6.61
MnO	0.10	0.07	0.07	0.19	0.07	0.08	0.08	0.14	0.10	0.11	0.08	0.09	0.17	0.03	0.14	0.15
MgO	4.34	5.45	5.16	4.82	5.60	4.47	4.75	3.58	5.42	5.37	5.17	5.12	4.89	3.82	4.63	4.67
CaO	7.24	6.64	6.57	12.37	7.22	9.81	9.41	10.25	10.04	7.04	8.82	8.58	5.94	4.49	9.54	8.39
Na_2O	2.10	1.56	1.14	1.62	1.26	0.76	0.97	0.96	1.33	1.56	1.60	1.54	1.86	1.35	1.32	1.28
K_2O	1.93	2.43	2.70	1.64	2.47	2.78	2.77	2.82	2.13	2.50	2.21	2.25	1.84	2.79	2.87	2.91
P_2O_5	0.26	0.29	0.26	0.74	0.46	0.22	0.13	0.41	0.48	0.28	0.35	0.30	0.18	0.25	0.20	0.40
L.O.I.	2.78	3.15	4.53	4.92	2.93	8.04	7.09	1.39	5.86	3.65	5.23	5.49	2.11	6.19	2.12	1.67
Tot	100	100	100	100	100	100	100	100	100	100	100	100	100	100	100	100

In order to validate the L.O.I. procedure on selected samples of mortar (from n. 9 to n. 17) bricks (samples 2 and 6) and clays (samples 18 and 19), calcimetric analyses were carried out (gas volumetric method) [25,26]. The carbonate content, if present, was determined on the basis of the chemical reaction between a known quantity of sample (0.500 g) and 10% hydrochloric acid (HCl) according to the following chemical reaction:

$$CaCO_3 + 2HCl \longrightarrow CO_2 + H_2O + CaCl$$

The percentage of calcium carbonate in each sample analyzed was calculated by measuring the quantity of carbon dioxide developed; for each mole of calcium carbonate, one mole of carbon dioxide is generally formed [27]. in the L.O.I. procedure, the loss of weight is due only to volatile elements. In the case of the presence of carbonate, the procedure is only able to measure the loss of CO_2. The latter corresponds to 43.971% (based on the molecular weight) of the calcium carbonate content. For this reason, the loss of weight recorded by the L.O.I. results in some cases should appear to be higher than the percentage of carbonates.

3. Results

All of the collected samples were subjected to particle size analysis and then XRF analysis for the characterization of the major elements and trace elements present in order to better discriminate the samples from each other.

3.1. Particle Size Analyses

According to Shepard [28], all mortar samples can be classified as sand. Figure 2a, in fact, shows that all of the samples analyzed were grouped in the lower-left part of the Clay–Sand–Silt triangle, representing sand samples.

The natural sediments (originally named as sand—see Table 1) showed a different grain-size distribution, as shown in the Clay–Sand–Silt triangle in Figure 2b: seven samples were silty sand (grouped in the yellow circle), five samples were sand (grouped in the orange circle), two samples were loam (grouped in the green circle), one could be classified as silty clay (green circle), and one could be classified as clayey sand (green circle). This variability had no correlation with the location in the excavation area but could be explained in terms of the sedimentological environment.

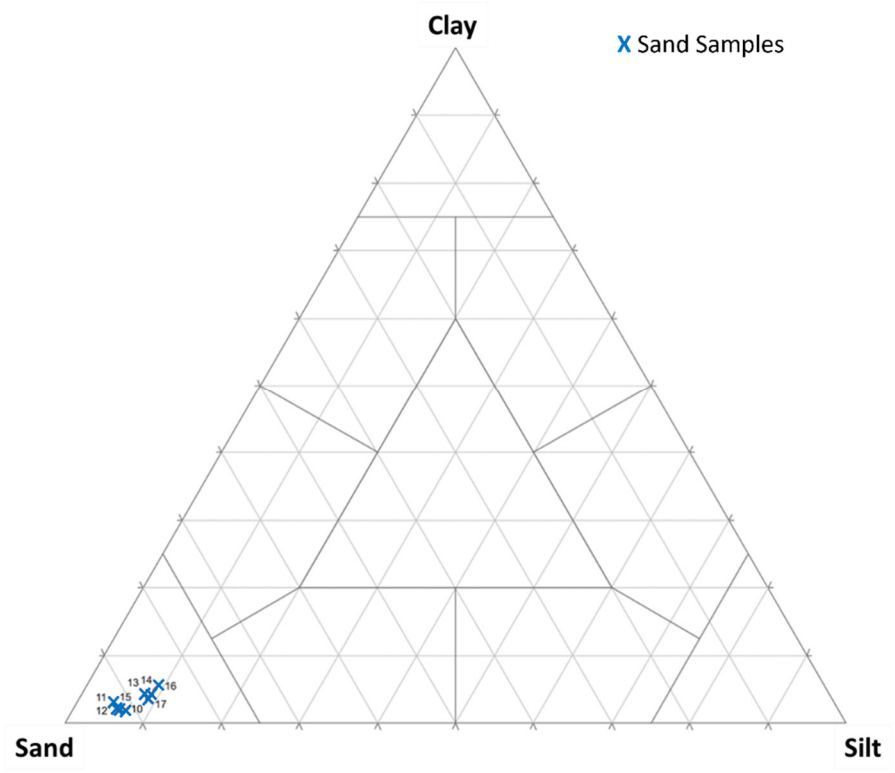

(**a**)

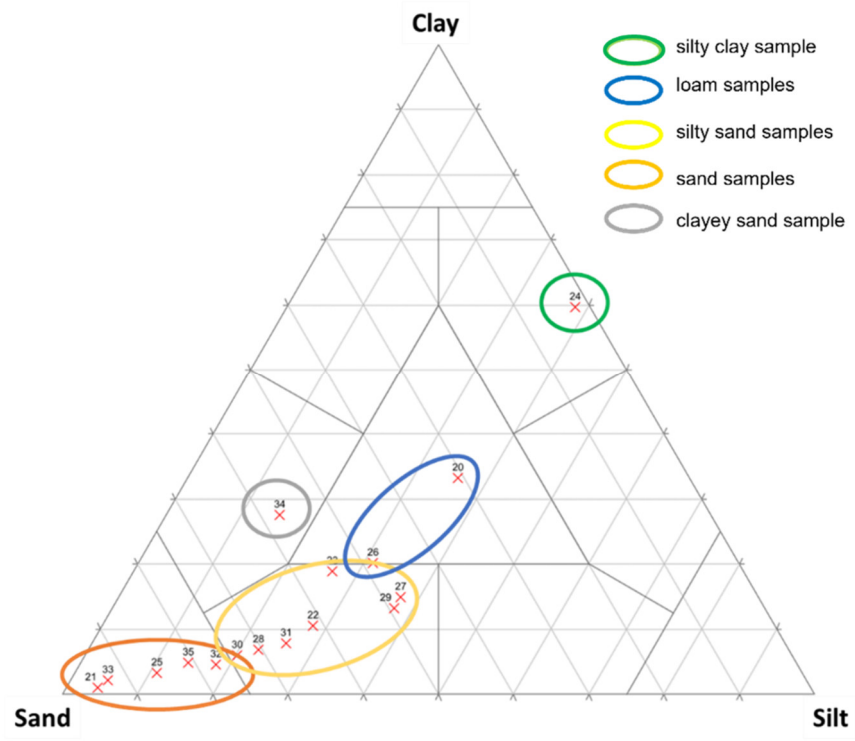

(**b**)

Figure 2. Classification according to Shepard [28] of: (**a**) mortar samples and (**b**) natural samples. The yellow circle represents the silty sand samples, the orange circle represents the sand samples, the blue circle represents the loam samples, the green circle represents the silty clay sample, and the gray circle represents the clayey sand sample.

3.2. XRF Analyses

The chemical composition (major and trace elements) of all of the samples collected was determined by XRF.

Table 2 and Figure 3 show the data relating to the chemical elements analyzed in the different samples for both the major elements expressed using the oxide concentration in the weight percentage and trace elements concentration expressed in ppm. In all of the samples, the oxides were characterized by high values of SiO_2, Al_2O_3, and CaO, followed by Fe_2O_3 and MgO.

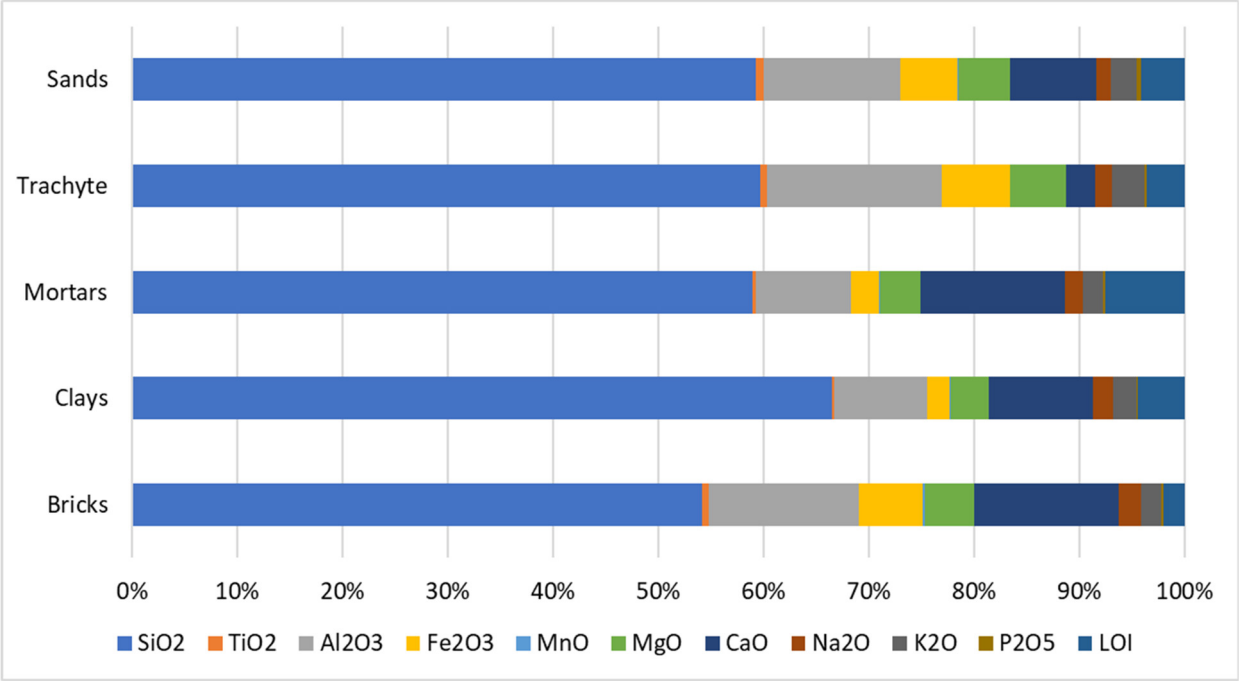

Figure 3. Bar chart showing the relative abundances of the major oxides in the different types of samples analyzed in this work. Each line represents the average value of those expressed in Table 2.

In addition to the tables, the chemical analyses of all samples were interpreted using binary diagrams of the variation in every single chemical element with respect to silica. In each diagram, the brick samples are colored in red, mortar samples in green, clay samples in yellow, trachyte samples in pink, and sand samples in blue.

Brick samples (colored in red in the diagrams of Figure 4) were generally characterized by a low value of silica with respect to the other samples, a high value of Al_2O_3 (Figure 4a), Fe_2O_3 (Figure 4b), MnO (Figure 4c), MgO (Figure 4d), CaO (Figure 4e), and Na_2O (Figure 4f), and more similar values of the trace elements, such as Co (Figure 4h) and Cr (Figure 4i), as shown in Table 2.

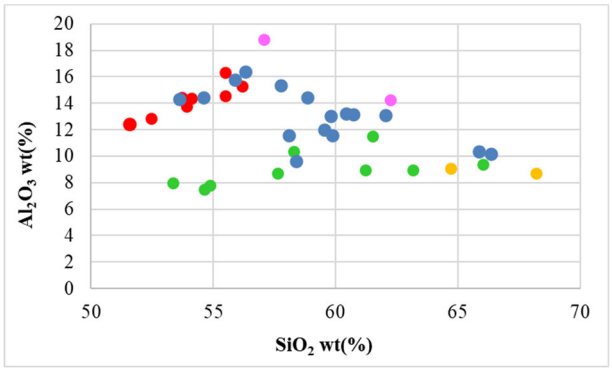
Al2O3 wt(%)
SiO2 wt(%)

(**a**)

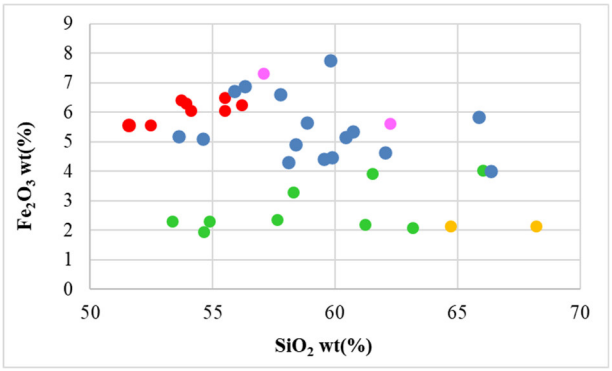
Fe2O3 wt(%)
SiO2 wt(%)

(**b**)

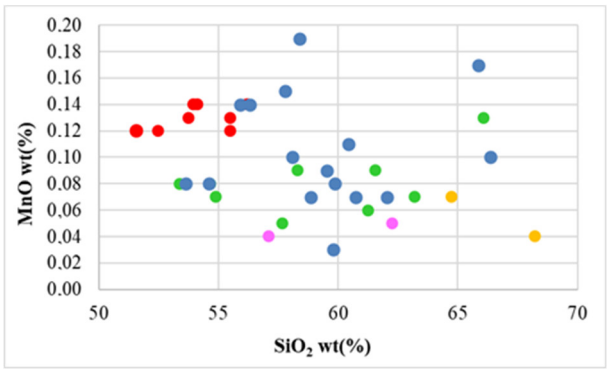
MnO wt(%)
SiO2 wt(%)

(**c**)

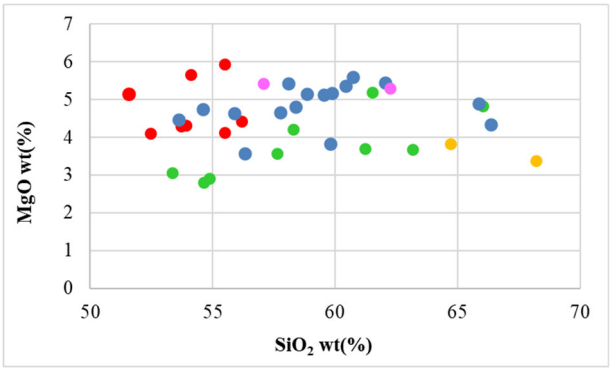
MgO wt(%)
SiO2 wt(%)

(**d**)

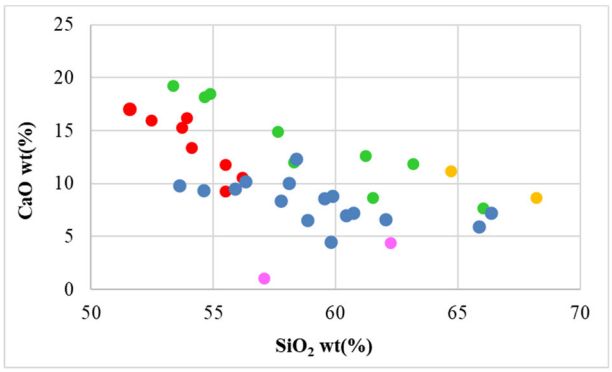
CaO wt(%)
SiO2 wt(%)

(**e**)

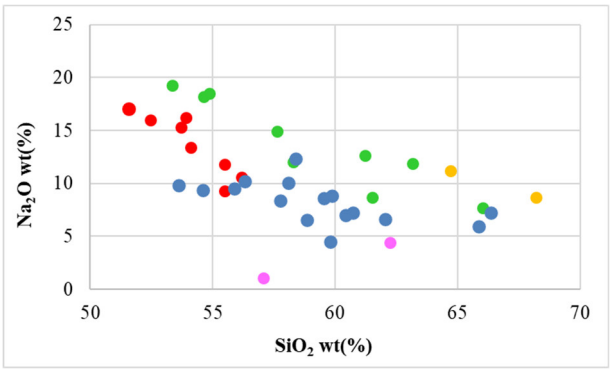
Na2O wt(%)
SiO2 wt(%)

(**f**)

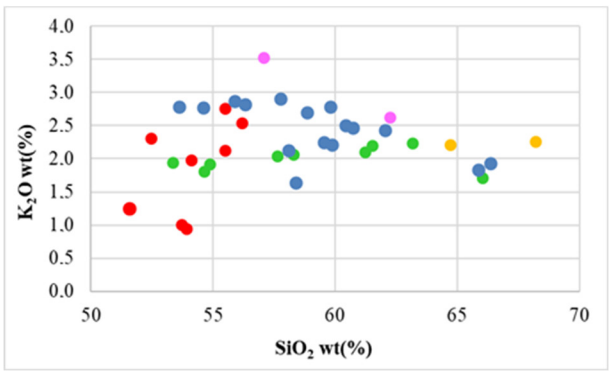
K2O wt(%)
SiO2 wt(%)

(**g**)

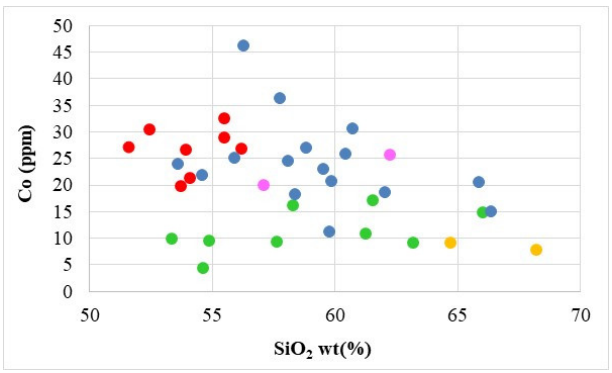
Co (ppm)
SiO2 wt(%)

(**h**)

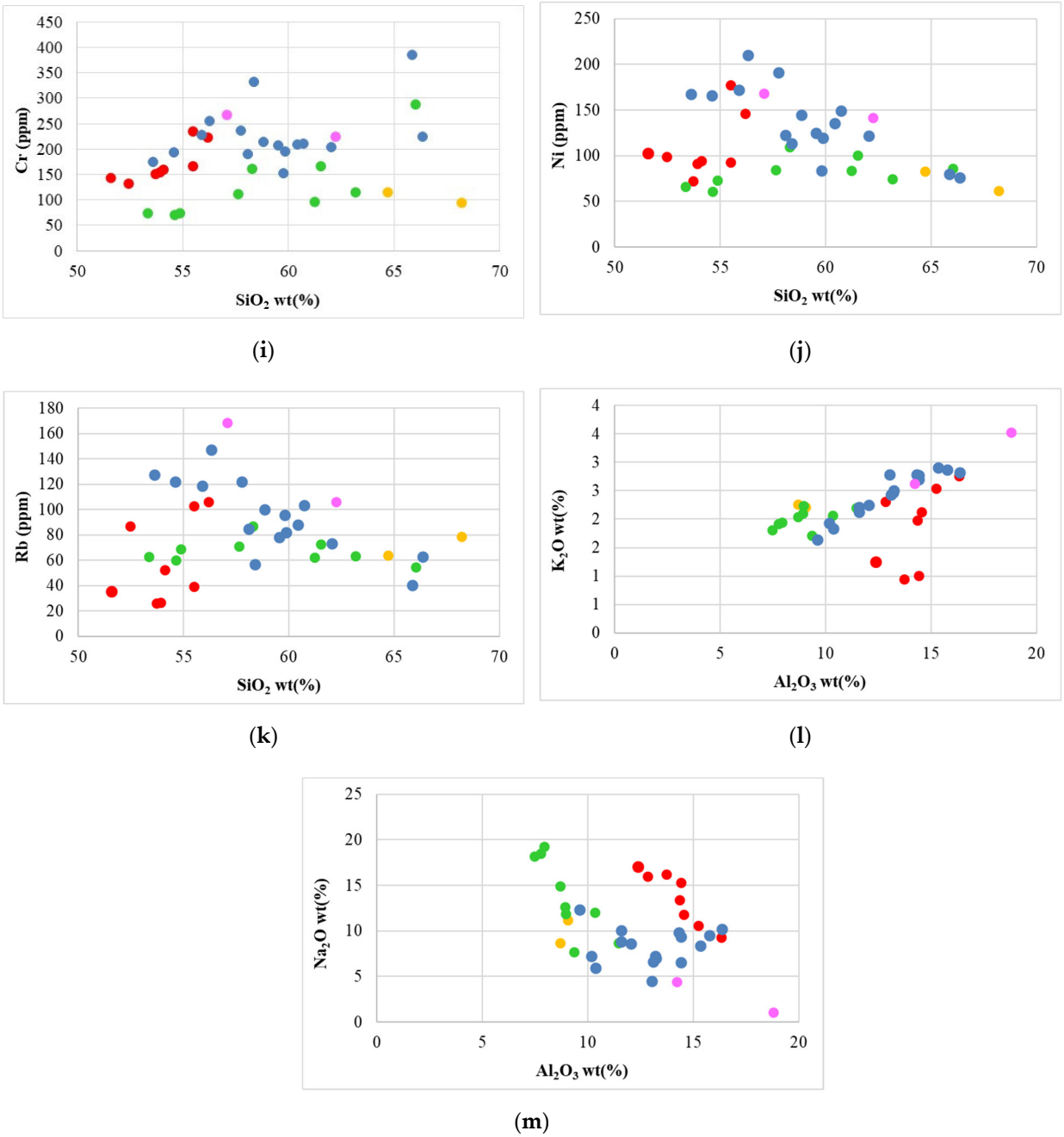

Figure 4. Binary diagrams between silica (SiO_2) and aluminum (Al_2O_3) and the major and minor elements obtained through XRF analyses and expressed in weight oxide (%) for the major elements and in ppm for minor elements: (**a**) SiO_2/Al_2O_3; (**b**) SiO_2/Fe_2O_3; (**c**) SiO_2/MnO; (**d**) SiO_2/MgO; (**e**) SiO_2/CaO; (**f**) SiO_2/Na_2O; (**g**) SiO_2/K_2O; (**h**) SiO_2/Co; (**i**) SiO_2/Cr; (**j**) SiO_2/Ni; (**k**) SiO_2/Rb; (**l**) Al_2O_3/K_2O; and (**m**) Al_2O_3/Na_2O. In each diagram, red spots represent the brick samples, yellow spots represent the clay samples, green spots represent the mortar samples, pink spots represent the trachyte samples, and blue spots represent the sand samples.

The opposite was observed for the clay samples (colored in yellow in the diagrams in Figure 4), with a higher value of silica but lower values of the other major oxides with respect to the brick samples and low values of the trace elements Co (Figure 4h), Cr (Figure 4i), and Ni (Figure 4j) (Table 2). The results obtained for both major and trace elements could have confirmed that the clay collected was not used to build the bricks.

Mortar samples (colored in green in the diagrams in Figure 4) showed low values of Al_2O_3 (Figure 4a), Fe_2O_3 (Figure 4b), and MgO (Figure 4d), similar to the clay samples, but

a high value of CaO (Figure 4e), as shown in Table 2, and similar to the brick samples (Table 2a). Regarding the trace elements, mortar samples were characterized by low values of trace elements, such as Co (Figure 4h), Cr (Figure 4i), Ni (Figure 4j), and Rb (Figure 4k), with respect to the other samples.

Table 2 also shows the XRF data obtained from the analyses of the trachyte samples, which were characterized by higher values of Al_2O_3 (Figure 4a), Fe_2O_3 (Figure 4b), MgO (Figure 4d), and K_2O (Figure 4g) and lower values of MnO (Figure 4c), CaO (Figure 4e), and Na_2O (Figure 4f). In the diagram in Figure 4, the trachyte samples are colored pink and show a high value of Rb in Figure 4k.

Finally, Table 2 shows the data obtained on the sand samples (colored in blue in the diagrams of Figure 4) with different values of silica (between 53.62–66.37), but generally low values of CaO and Na_2O.

In geochemical analysis, L.O.I. represents the H_2O released by clay and gypsum minerals, as well as the CO_2 released by calcite and dolomite. Mortar samples were enriched in calcite and dolomite, and showed higher values of L.O.I. and carbonate contents. Regarding the brick samples, they presented lower values of L.O.I. compared with the mortars, and also lower carbonate content values, which was in accordance with their technological condition in which the clay minerals dissociated during the firing process; the carbonate content values can be attributed to the smear used in the mixture. Finally, calcimetric analyses of the two clay samples showed different carbonate contents.

3.3. Calcimetry Analyses

Regarding the characterization of the mortar samples, there was a strong affinity between these samples and the sand samples, which could indicate a local source, probably in the Po delta area. The compositional variation that was observed was probably linked to the addition of lime, which suggested the use of sediments similar to the paleo-channel environments for the samples collected at the base of the second wall structure. The characterization of the mortar samples was conducted by calcimetric analysis. Figure 5 shows a selection of highly classified mortars, possibly from neighboring paleo-dune areas. Samples 9, 10, 11, 15, and 16 showed the same values as the percentages changed (1%, 2%, and 3%); consequently, the average percentage corresponded to the same value. With respect to the other, only sample 17 showed a lower calcimetric value, but it remained constant as the percentage changed.

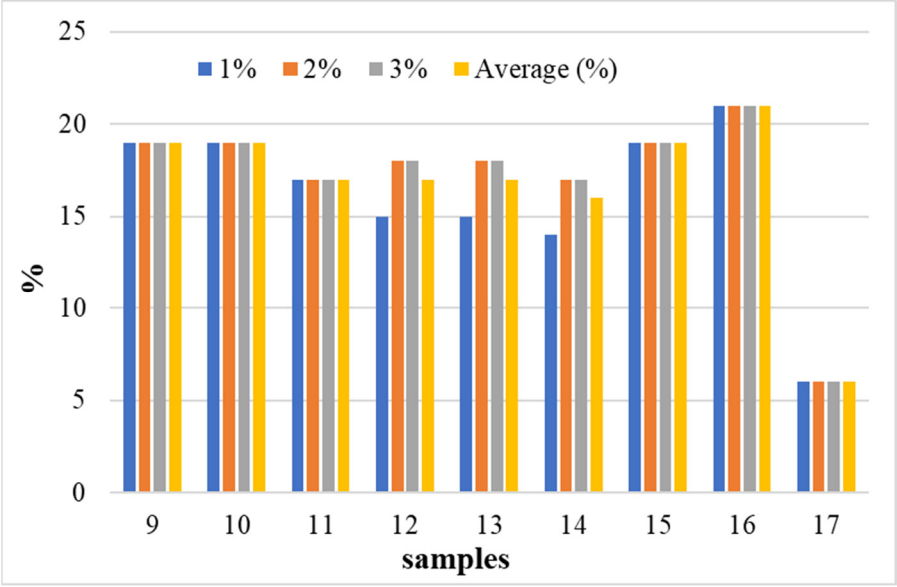

Figure 5. Data obtained by the calcimetry analyses of mortar samples. The blue color represents 1%, the orange color represents 2%, the gray color represents 3%, and the yellow color represents the average expressed in percentage.

4. Discussion

From the study of the XRF analyses of the coarser fractions of sandy sediments obtained through sedimentological analyses, an almost absent correlation between SiO_2 and Al_2O_3 (Figure 4a), MgO (Figure 4d), and K_2O (Figure 4g) was observed, which could be related to different abundances of minerals, such as quartz, feldspars, and micas.

An important environmental indicator was the different trends of alkaline elements (especially K_2O and Rb) compared with SiO_2. In the binary diagrams, the sand samples showed a decrease in K_2O (Figure 4g) and Rb (Figure 4k) as SiO_2 increased. In addition, a low value of MnO, which characterized all sand samples (Figure 4f), between 0.03 and 0.15 could indicate that sedimentation occurred at times when mature soils were not yet developed through pedogenesis. This could mean that deforestation in the Roman centuriation did not result in the typical enrichment of all floodplains where agricultural activity was important. It can, therefore, be assumed that, despite the value of MgO in these sediments, the concentration of magnesium was severely depleted compared with the current concentrations in the Po Valley sediments [9], both for the sand samples and also for the bricks for which this material probably represented one of the main raw materials [11].

Regarding the brick samples, it must be considered that brick production reached almost industrial importance in the Po Delta area between the first century B.C. and the first century A.D., as confirmed both by literary sources [12] and by the very high number of archaeological finds. It should not be forgotten that the Pansiana brickworks operated in this area, and one of its products was stamped tiles. The Pansiana workshop was active in the Delta area, chronologically placed between the end of the Republican and Flavian periods and supported, above all, by findings in the area of San Vito and on the Argine d'Agosta (Comacchio) [29]. The imperial heritage of the Pansiana figlina was linked to C. Vibius Pansa Caetronianus, consul in 43 B.C. and governor of Cisalpine Gaul in 45 B.C. [30]. The entire Adriatic coast, within Cisalpine Gaul and especially on the Adria–Rimini line, was characterized by the presence of materials from this workshop, which later became the property of the emperor Augustus. For this reason, one could hypothesize that the Pansiana figlina was located near the Fossa Augusta due to the waste from the kiln and production facilities found at Argine d'Agosta [31].

With regard to the brick samples found and considered in this work, it was assumed that the structure was built from calcium-rich bricks (as evidenced by the SiO_2/CaO graph in Figure 4e). The presence of calcium carbonate in the mixture afforded the material greater porosity [32] and the firing product was, therefore, lighter. During the firing process, the dissociation of the calcium carbonate released CO_2, which produced bubbles within the mixture. In addition, CO_2 could act as an inhibitor in the oxidation processes of iron, which is why the bricks produced often tended to have a lighter, almost albasious coloring [12].

On the other hand, the bricks used to build the lighthouse tower had to be dense and heavy, massive, and have good physical–mechanical properties; therefore, they were produced from clay low in calcium carbonates.

5. Conclusions

This research, based on a mineralogical–petrographic and geochemical approach, permitted the provision of preliminary data regarding the characterization of the excavation context and the construction materials found.

Geochemical analyses showed that clay samples of the lighthouse tower in Comacchio were obtained from basins poor in carbonates, while, for the construction of

the bricks of the second wall structure, clays rich in carbonate were chosen to afford lightness to the structure resting on a wooden grid.

Granulometric analyses highlighted the fact that the depositional environments were of a very different nature: natural sediments, mainly consisting of sands and silty sands, were suggested to be related to a fluvial environment with some intercalations of finer deposits due to a variable fluvial dynamic; and sands were attributable to a paleo–alveo environment.

During the 2015 campaign, trachyte samples were also found, an effusive magmatic rock coming from the Euganean Hills in the province of Padua commonly used in the Roman ages to pave the main communication routes. Only further analyses, hopefully, connected to the reopening of the excavation and the consequent enlargement of the area to be investigated will be able to provide more precise details.

Author Contributions: Conceptualization, E.M., C.T., M.C., M.B. and C.V.; methodology, E.M., C.T., U.T. and C.V.; formal analysis, E.M. and U.T.; investigation, E.M., C.T. and C.V.; resources, C.V.; data curation, E.M., C.T., U.T, M.C., M.B. and C.V.; writing—original draft preparation, E.M., C.T. and U.T.; writing—review and editing E.M., C.T., U.T., M.C. and C.V.; visualization, E.M. and C.T.; supervision, E.M., U.T. and C.V.; project administration, C.V.; funding acquisition, C.V. All authors have read and agreed to the published version of the manuscript.

Funding: This research received no external funding.

Institutional Review Board Statement: Not applicable.

Informed Consent Statement: Not applicable.

Data Availability Statement: Not applicable.

Acknowledgments: The authors wish to thank the director of the Superintendence of Archaeology, Fine Arts, and Landscape for the enhancement of the widespread archaeological heritage of the Po delta area for helping us in our research.

Conflicts of Interest: The authors declare no conflict of interest.

References

1. Liritzis, I.; Laskaris, N.; Vafiadou, A.; Karapanagiotis, I.; Volonakis, P.; Papageorgopoulou, C. Archaeometry: An overview. *Sci. Cult.* **2020**, *6*, 49. https://doi.org/10.5281/zenodo.3625220.
2. Pecci, A.; Nizzo, V.; Bergamini, S.; Reggio, C.; Vidale, M. Residue analysis of late Bronze Age ceramics from the archaeological site of Pilastri di Bondeno (northern Italy). *Preist. Alp.* **2017**, *49*, 51–57.
3. Marrocchino, E.; Telloli, C.; Caraccio, S.; Guarnieri, C.; Vaccaro, C. Medieval Glassworks in the City of Ferrara (North Eastern Italy): The Case Study of Piazza Municipale. *Heritage* **2020**, *3*, 819–837. https://doi.org/10.3390/heritage3030045.
4. Pérez-Monserrat, E.M.; Causarano, M.A.; Maritan, L.; Chavarria, A.; Brogiolo, G.P.; Cultrone, G. Roman brick production technologies in Padua (Northern Italy) along the Late Antiquity and Medieval Times: Durable bricks on high humid environs. *J. Cult. Herit*. **2022**, *54*, 12–20. https://doi.org/10.1016/j.culher.2022.01.007.
5. Olavarría, C.P.; Castro de Machuca, B. Petrographic characterization and identification of temper sources in local ceramics during the Inca domination and early Spanish colony (Mendoza, west-central Argentina). *J. Archaeol. Sci. Rep.* **2017**, *13*, 351–360. https://doi.org/10.1016/j.jasrep.2017.04.011.
6. Ntah, Z.L.E.; Sobott, R.; Fabbri, B.; Bente, K. Characterization of some archaeological ceramics and clay samples from Zamala—Far-northern part of Cameroon (West Central Africa). *Cerâmica* **2017**, *63*, 413–422. https://doi.org/10.1590/0366-69132017633672192.
7. Dalkiliç, N.; Nabikoğlu, A. Traditional manufacturing of clay brick used in the historical buildings of Diyarbakir (Turkey). *Front. Archit. Res.* **2017**, *6*, 346–359. https://doi.org/10.1016/j.foar.2017.06.003.
8. Rautureau, M.; Figueiredo Gomes, C.S.; Liewig, N.; Katouzian-Safadi, M. Clay and Clay Mineral Definition. In *Clays And Health*; Springer: Cham, Switzerland, 2017; pp. 5–31. https://doi.org/10.1007/978-3-319-42884-0_2.
9. Marrocchino, E.; Telloli, C.; Vaccaro, C. Geochemical and Mineralogical Characterization of Construction Materials from Historical Buildings of Ferrara (Italy). *Geosciences* **2021**, *11*, 31. https://doi.org/10.3390/geosciences11010031.
10. Maselli, V.; Pellegrini, C.; Del Bianco, F.; Mercorella, A.; Nones, M.; Crose, L.; Guerrero, M.; Nittrouer, J.A. River Morphodynamic Evolution under Dam-Induced Backwater: An Example from the Po River (Italy). *J. Sediment. Res.* **2018**, *88*, 1190–1204. https://doi.org/10.2110/jsr.2018.61.
11. Ugolini, F. Pliny the Elder, Paolo Armileo and the Antiquarian Reception of the Portus Augusti Ravennatis. *Int. Class. Trad.* **2020**, *27*, 513–530. https://doi.org/10.1007/s12138-019-00527-1.

12. Marrocchino, E.; Telloli, C.; Cesarano, M.; Montuori, M. Geochemical and petrographic characterization of bricks and mortars of the parish church Santa Maria in Padovetere (Comacchio, Ferrara, Italy). *Minerals* **2021**, *11*, 530. https://doi.org/10.3390/min11050530.
13. Gelichi, S.; Grandi, E.; Negrelli, C. *Un Emporio e la sua Cattedrale: Gli Scavi di Piazza XX Settembre e Villaggio San Francesco a Comacchio*; All'Insegna del Giglio: Sesto Fiorentino FI, Italy, 2021.
14. Corbau, C.; Zambello, E.; Rodella, I.; Utizi, K.; Nardin, W.; Simeoni, U. Quantifying the impacts of the human activities on the evolution of Po delta territory during the last 120 years. *J. Environ. Manag.* **2019**, *232*, 702–712. https://doi.org/10.1016/j.jenvman.2018.11.096.
15. Da Lio, C.; Tosi, L. Vulnerability to relative sea-level rise in the Po river delta (Italy). *Estuar. Coast. Shelf Sci.* **2019**, *228*, 106379. https://doi.org/10.1016/j.ecss.2019.106379.
16. Kay, S.; Pomar, E.; Hay, S. Spina revisited: The 2008 geophysical prospection in the light of the excavation results. *Groma* **2020**, *5*, 1–16. https://doi.org/10.12977/groma35.
17. Akaaza, J.N.; Bam, S.A.; Iortsor, A. Investigation of the Properties of Makurdi, Buruku and Katsina-Ala Silica Sand Deposits for Glass Production. *Taraba J. Eng. Technol.* **2018**, *1*, 80–83.
18. Saccani, E. *Petrografia Delle Rocce Sedimentarie Terrigene*; Università degli Studi di Ferrara: Ferrara, Italy, 2014.
19. Wentworth, C.K. A Scale of Grade and Class Terms for Clastic Sediments. *J. Geol.* **1922**, *30*, 377–392. https://doi.org/10.1086/622910.
20. Folk, R.L.; Ward, W.C. Brazos River bar: A study in the significance of grain size parameters. *J. Sediment. Petrol.* **1957**, *27*, 3–26. https://doi.org/10.1306/74D70646-2B21-11D7-8648000102C1865D.
21. Marrocchino, E.; Telloli, C.; Vaccaro, C. Microscopic and chemical characterization of metal slags found at the Porta Paola excavation in Ferrara. In Proceedings of the 2020 IMEKO TC-4 International Conference on Metrology for Archaeology and Cultural Heritage, Trento, Italy, 22–24 October 2020.
22. Marrocchino, E.; Telloli, C.; Pedrini, M.; Vaccaro, C. Natural stones used in the Orsi-Marconi palace façade (Bologna): A petro-mineralogical characterization. *Heritage* **2020**, *3*, 1109–1124. https://doi.org/10.3390/heritage3040062.
23. Marrocchino, E.; Telloli, C.; Leis, M.; Vaccaro, C. Geochemical-Microscopical Characterization of the Deterioration of Stone Surfaces in the Cloister of Santa Maria in Vado (Ferrara, Italy). *Heritage* **2021**, *4*, 2996–3008. https://doi.org/10.3390/heritage4040167.
24. Marrocchino, E.; Telloli, C.; Novara, P.; Meletti, V.; Vaccaro, C. Petro-archaeometric characterization of historical mortars in the city of Ravenna (Italy). In Proceedings of the 2020 IMEKO TC-4 International Conference on Metrology for Archaeology and Cultural Heritage, Trento, Italy, 22–24 October 2020.
25. Tang, L. Gas capacity method to determine the content of bicarbonate and carbonate in sodium silicate sand. *IOP Conf. Ser. Earth Environ. Sci.* **2018**, *170*, 022159. https://doi.org/10.1088/1755-1315/170/2/022159.
26. Rosselli, G.; Mirabile Gattia, D.; AlShawa, O.; Cinaglia, P.; Di Girolami, G.; Francola, C.; Persia, F.; Petrucci, E.; Piloni, R.; Scognamiglio, F.; et al. Mortar analysis of historic buildings damaged by recent earthquakes in Italy. *Eur. Phys. J. Plus* **2019**, *134*, 540. https://doi.org/10.1140/epjp/i2019-13024-2.
27. Dashtgard, S.E.; Wang, A.; Pospelova, V.; Wang, P.L.; La Croix, A.; Ayranci, K. Salinity indicators in sediment through the fluvial-to-marine transition (Fraser River, Canada). *Sci. Rep.* **2022**, *12*, 14303. https://doi.org/10.1038/s41598-022-18466-4.
28. Shepard, F.P. Nomenclature based on sand-silt-clay ratios. *J. Sediment. Petrol.* **1954**, *24*, 151–158; https://doi.org/10.1306/D4269774-2B26-11D7-8648000102C1865D.
29. Zamboni, L.; Cesarano, M.; Bruni, M. La villa rustica di Alberone di Ro (FE), località Ca' Nova. Scavi 2010–2015. In *Antichi romani e Romanità Nelle Terre del Delta del Po: Nuovi Studi e Prospettive di Ricerca*; AnteQuem: Barcelona, Spain, 2018.
30. Maritan, F.E. I laterizi iscritti di epoca romana rinvenuti nel crollo del campanile di San Marco: Nuovi dati da vecchi scavi. In *Atti del Convegno Internazionale*; Pietre di Venezia: Spolia in sé, spolia in re; L'Erma: Venezia, Italy, 2015; pp. 195–209.
31. Rucco, A.A. *Comacchio nell'alto Medioevo: Il Paesaggio tra Topografia e Geoarcheologia*; All'Insegna del Giglio: Sesto Fiorentino, Italy, 2015.
32. Cultrone, G.; Aurrekoetxea, I.; Casado, C.; Arizzi, A. Sawdust recycling in the production of lightweight bricks: How the amount of additive and the firing temperature influence the physical properties of the bricks. *Constr. Build. Mater.* **2020**, *235*, 117436. https://doi.org/10.1016/j.conbuildmat.2019.117436.